*Express Polymer Letters Vol.19, No.1 (2025) 3–14*
*Available online at www.expresspolymlett.com*
*https://doi.org/10.3144/expresspolymlett.2025.2*

*Research article*

# Surface texture effects on mechanical properties of additively manufactured polylactic acid

*Emir Avcioglu*[*]

Hitit University Mechanical Engineering Department Corum, Turkey

*Received 2 August 2024; accepted in revised form 3 October 2024*

**Abstract.** Additive manufacturing is favored for its capacity to create intricate geometries and enhance component functionality more efficiently than traditional methods. Applying texture to materials is one of the processes used to add functionality to products, wherein it can improve adhesion and tribological behavior in biomedical applications while also controlling mechanical properties and providing perceptual and aesthetic improvements. In this study, custom black-white images containing vertical lines were prepared and added as textures to the design of tensile test specimens during slicing. Custom textured and untextured tensile test specimens were fabricated using the Fused Deposition Method with polylactic Acid filament to evaluate the effect of texture parameters, such as protrusion offset (0.25, 0.50, 0.75 mm), number of protrusions (3, 6) and infill pattern (rectilinear, line, concentric), on the tensile strength of the specimens. Through the analysis of tensile test results and examination of microscopic and slicing software images, it was found that texturing resulted in a reduction in ultimate tensile strength due to nozzle trajectory deviations and stress concentration. The least detrimental texturing parameters observed in this study were 0.5 mm protrusion offset and 3 protrusions with concentric and line infill patterns, resulting in a reduction in tensile strength of 2.36 and 5.79%, respectively when compared to untextured specimens.

***Keywords:*** *surface texturing, polylactic acid, mechanical properties, additive manufacturing, biocompatible polymer*

## 1. Introduction

In recent years, the adoption of additive manufacturing has proliferated due to the decreasing costs of equipment and consumables, coupled with the expanding variety of available technologies. The fundamental principle of additive manufacturing is rooted in the digital slicing of a material's solid model, using specialized software, and subsequently depositing materials in solid or liquid form, layer by layer. Material extrusion technology (MEX), which includes methods such as pellet extrusion, powder extrusion, and fused filament fabrication (FFF), has been widely adopted over the last decade [1]. In this approach, a polymer in pellet, powder, or filament form is extruded through the nozzle after reaching its melting temperature. Among these, the FFF technique, based on depositing polymer in filament form, has proven to be a prominent prototyping method due to its cost-effectiveness and the diversity of available equipment and consumables [2]. In this approach, a polymer in filament form, typically with a diameter of 1.75 or 2.85 mm, is extruded through the nozzle after reaching its melting temperature. The nozzle then moves across the table according to the generated G-codes, depositing the molten polymer layer by layer until the desired geometry is obtained [3]. In FFF production, polymers with varying properties, including polylactic acid (PLA), acrylonitrile butadiene styrene (ABS), polyethylene terephthalate glycol (PETG), thermoplastic polyurethane (TPU) and polyamide (PA) are utilized to meet the desired mechanical requirements. Among these polymers, PLA stands out as a prevailing choice for rapid prototyping due to its ease of printing, cost-effectiveness, and

[*]Corresponding author, e-mail: emiravcioglu@hitit.edu.tr

compatibility with most standard 3D printers [4]. Furthermore, the biocompatibility and biodegradability of PLA are driving extensive production and heightened research efforts in this domain. The extensive utilization of PLA, along with certain drawbacks, has motivated researchers to conduct more comprehensive investigations in this field. Efforts are presently underway in this domain to address challenges, including suboptimal surface quality, limited production capacity due to the small printer table, and relatively low mechanical properties [5]. Research and development activities, such as the optimization of printing parameters, post-manufacturing processes, polymer development, and the incorporation of reinforcement materials into polymers, are underway to address these drawbacks [6]. The modifications in product properties resulting from variations in printing parameters, materials, and post-production processes are determined through testing procedures conducted in accordance with the relevant standards.

Additive manufacturing holds a key advantage in its capability to fabricate intricate geometries and apply texturing to material surfaces. This technological process enables the production of highly intricate and customized designs, allowing for enhanced structural complexity and surface manipulation. Surface textures serve both aesthetic and functional purposes as they are deliberately introduced on product surfaces [7]. One of the primary motives for introducing surface textures with aesthetic intentions is to impart a sophisticated visual complexity to the external surfaces. For instance, this may involve the deliberate modification of exterior surfaces, such as those in vehicle interior plastics, to enhance adhesion characteristics. Texturing on additively manufactured components for functional purposes was initially suggested within the context of biomedical applications. Notably, these surface patterns were observed to enhance the adherence of orthopedic implants to biological tissues [8].

The proliferation of texturing applications in additive manufacturing is advancing in tandem with the evolving software development within this specific domain. Through the application of surface texturing, Hong *et al*. [9] demonstrated the attainment of reduced or enhanced friction coefficients, as well as the emergence of tribological behaviors inspired by biological principles in plastic parts. Similarly, Holovenko *et al*. [10] achieved analogous results in their investigation of metal parts. In the research conducted by Jafari *et al*. [11], it was demonstrated that textures generated through high-resolution additive manufacturing processes exerted precise control over surface wettability, approaching a superhydrophobic behavior. Research findings indicate that appropriately designed surface textures can lead to enhancements in structural properties. For instance, Ko *et al*. [12] demonstrated that Voronoi-like patterns contributed to an increase in the flexural strength of plastic components. Johnson *et al*. [13] observed an augmented resistance to blade penetration associated with surface textures featuring bioinspired patterns. In research endeavors aimed at managing the perceptual and aesthetic attributes of additive manufacturing products, Mai *et al*. [14] generated grain patterns on plastic components to replicate the visual and tactile characteristics associated with wooden furniture. In research conducted by Ou *et al*. [15], hair-like patterns were designed on plastic components, serving dual objectives of ornamentation and enhancement of tactile perception. Van Rompay *et al*. [16] introduced regular patterns on the cups, and their findings indicated that these patterns had a positive impact on the perceived quality of the beverage held within the cup.

In practice, the application of surface patterns can typically be incorporated during the design phase or subsequently during the slicing process following the initial design. In the study conducted by Maekawa *et al*. [17], auto-correlated random patterns characterized by $1/f$ fluctuations were employed as a design element on standard tessellation language (STL) models to achieve decorative effects on additive manufacturing components. In the work of Armillotta [18], basic patterns generated through mathematical equations were incorporated into flat specimens for the purpose of evaluating the detail resolution of a particular additive manufacturing process. Partially automated texturing methods have been suggested for surfaces of moderate complexity. In the study conducted by Jee and Sachs [19], the texture is initially defined on a parametric surface patch, and subsequently, an interactive mapping process is employed to apply this texture to a specific area of the triangle mesh. In the research by Zhou *et al*. [20], a pattern originally defined on a curve is transposed onto a 3D model through the application of interactively generated geometry. This methodology allows for the incorporation of the textured model with other components to achieve intricate and manufacturable assemblies. In the study conducted by Dumas *et al*. [21], a prototypical texture is meticulously emulated by engraving a pattern onto the surface of a part. This method involves the projection of texture images from randomly oriented planes surrounding the part onto a voxel structure on the part's surface. The selection of the optimal plane for each voxel is edited to maximize the fidelity of the replicated texture to the input design. Process-level strategies have been postulated for the inclusion of uncomplicated textures onto triangle meshes, regardless of their complexity. In the research by Kobayashi and Shirai [22], a periodic pattern is introduced onto a computer numerical control-machined part during the generation of toolpaths. This is achieved by arranging the assembly of spiral toolpaths generated over fundamental shapes obtained through the segmentation of the initial pattern. A preliminary stage within the additive manufacturing workflow, as delineated by Yaman *et al*. [23], involves the transformation of slicing contours into binary images. Subsequently, these binary images undergo modification via morphological operations designed to accommodate regular patterns. Texture mapping, a fundamental technique in 2D texturing, as outlined by Weinhaus and Devarajan [24], involves the process of choosing or interpolating colors from a digital image to acquire a specific pattern. In this research, the implementation of textures on the model was achieved through the utilization of slicing software. The software facilitates the transference of a black-and-white image to the model by effecting indentations and protrusions contingent upon the varying shades of black. The dimensions of these indentations and protrusions on the model are tailored in accordance with the color tones present in the image, the pattern composition, and the configurations established within the slicing software. Subsequently, for the purpose of reproducing the designed pattern, the slicing software undertakes the modification of the G-code, assigning tailored contours. Despite the existence of black-and-white patterns in the software library, the presence of tonal variations results in noise. Therefore, textures featuring vertical black lines were generated using Python and subsequently applied to the tensile sample in accordance with ASTM-D638 standard. Type-IV specimens, following ASTM D638 standards, were manufactured from PLA, each varying in the number of vertical patterns, size of protrusions, and varying infill patterns. In this investigation, an examination was conducted to assess the impact of varying these parameters on mechanical properties. The adoption of surface texturing across various product applications is expanding, yet research examining its impact on product mechanical properties remains scarce. This study seeks to identify the optimal texture dimensions and production parameters.

## 2. Experimental

### 2.1. Printing parameters and tests

In the context of 3D printing, the trajectory of the nozzle is governed by G-codes. The translation of the digital design into tangible form, aligned with predefined production parameters, is achieved through slicing software, resulting in the generation of G-codes. In the additive manufacturing process, wherein the material is consolidated into a cohesive structure, the external contours of the resulting object are shaped by the material walls. Meanwhile, the internal configuration is delineated by the application of distinct printing patterns and densities, tailored to achieve desired strength properties. Notable examples of infill patterns include grid, rectilinear, honeycomb, triangle, cubic, concentric, gyroid, and lines. On the other hand, there are three most common types of top/bottom patterns: Rectilinear (zigzag), line, and concentric. In this research, to maintain consistency between the top/bottom pattern and the infill pattern, rectilinear, line, and concentric infill patterns and top/bottom patterns were used. The samples were printed according to the ASTM D638 standard (Type-IV) with 100% infill density. PLA filaments with a diameter of 1.75 mm were used for printing purposes utilizing the Creality Ender 5 Pro 3D printer, which has a 0.4 mm diameter nozzle. To ensure high-quality prints with different filaments and printers, it's crucial to calibrate and optimize printing parameters through initial testing. Specialized 'calibration towers' are available as add-ons for this optimization process. These towers vary specific parameters at set intervals, allowing for the identification of the optimal settings for each print. In this study, speed towers, temperature towers, flow towers, and retraction towers were utilized to determine the ideal printing parameters. The determined printing parameters pertinent to product properties and meticulously maintained throughout the production process include nozzle temperature set at 215 °C, table temperature at 50 °C, layer height maintained at 0.2 mm, line width fixed at 0.4 mm, wall line count set to 4, and printing speed regulated at 40 mm/s.

Doseer stereo microscope was employed to take microscopic image to analyse the failure mechanism of the specimens after the tensile test.

According to the relevant tensile test standard, five samples were produced for each case. Protrusions and sample geometry were measured using digital calliper after production. The geometric accuracy of samples designed and produced by the FFF method depends on several factors, including layer thickness, extrusion temperature, part orientation, stepper motor sensitivity, filament diameter accuracy, and filament content; generally, a tolerance of ±0.1 mm and ±1% can be achieved on well-calibrated commercial printers [25]. In this study, by optimizing the printing parameters, samples were produced with an average tolerance of 1.1%.

Tensile tests were carried out using Shimadzu Universal Testing Machines in accordance with the relevant standard. Tensile tests were conducted using parameters such as a testing speed of 5 mm/min, chosen to comply with ASTM D638 standards.

## 2.2. Imparting texture

The first step in manufacturing using FFF is to create a solid model of the object using computer-aided design (CAD) software. This solid model is saved in either STL or 3MF format for use in slicing software. The 3MF format file contains metadata, including the solid model, color, material, and texture, whereas STL files contain only the 3D geometry of the model represented by a mesh of triangles. The slicing software processes this file by dividing it into thin layers that can be produced on a 3D printer and generates G-code. This G-code determines the movement of the extruder and build platform along the *X*, *Y*, and *Z* axes, the amount of filament extruded, nozzle and build platform temperatures, nozzle speed and retractions, and operation of the fan. The G-code file is then transferred to the printer to commence the printing process. Most slicing programs are available for free, each with its own set of advantages and disadvantages.

IdeaMaker was used as a slicing software because of its ability to apply customized texture to the vertical surfaces of a specimen. The process involves the controlled movement of the printing nozzle along the *Y*-axis to effectuate protrusions of predetermined dimensions and spatial positioning, synchronized with the lateral motion of the nozzle along the *X*-axis. The process involves the customization of G-codes along the *X* and *Y* axes to impart a bespoke texture onto the initially untextured solid model. This manipulation results in an alteration of the morphology of the specimen's vertical outer surface from its original state and influences the trajectory of the wall and infill pattern within the specimen as shown in the figure below. Figure 1 shows the application of texture

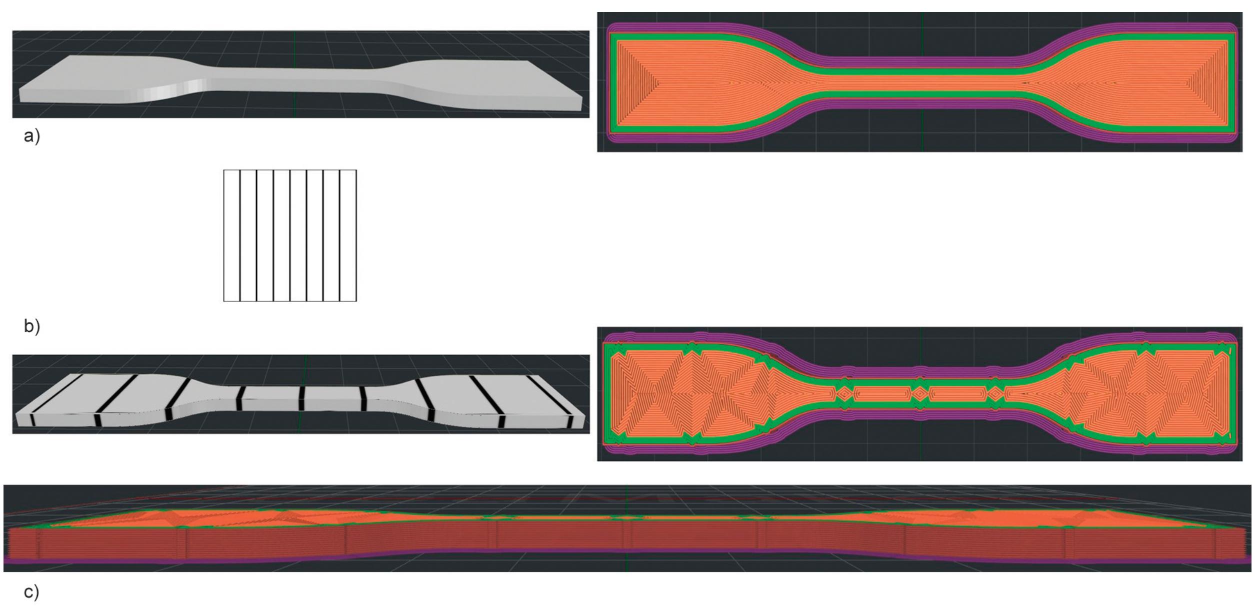


**Figure 1.** Imparting of the texture a) STL version of the sample b) vertical pattern c) vertical pattern imparted version of the sample.

onto the tensile specimen and its consequential impact on the trajectory adjustment of the printing nozzle within the sliced version of the specimen. Figure 1a illustrates the original STL model of the sample, Figure 1b displays the applied vertical pattern, and Figure 1c presents the resulting pattern imparted onto the sample. Within this representation, the purple hue signifies the brim, the dark orange delineates the outermost wall, the green hue represents the shell layers, while the orange hue illustrates the filling pattern.

To pattern the surface of the products, in other words, to create a tailored contour, first, evenly spaced black vertical lines were generated in the form of an image file using Python software. The number of protrusions on the tensile specimen was determined in this step. In this study, specimens with 3 and 6 protrusions in the area between the tensile jaws were produced. During slicing, the 'texture *XY* Offset' parameters were set at 0.25, 0.50, and 0.75 mm, determining the extent of texture protrusion. While selecting these protrusion values, preliminary tests were conducted, and slicer limitations were considered. In the slicer software, the protrusion offset is limited to 1 mm, as offsets beyond 0.75 significantly alter the geometry. Therefore, the offset values were selected as 0.25, 0.50, and 0.75 mm. Similarly, more than 6 protrusions cause significant changes in geometry; hence, 3 and 6 protrusions were selected.

### 2.3. Nozzle trajectories

The nozzle path during additive manufacturing is generated by slicing software based on the geometry and production parameters. Slicing images for each case were captured from the relevant software and tabulated to illustrate the nozzle trajectory. The following tables demonstrates the impact of different numbers and offsets of protrusions on the resulting contours, which represent the nozzle trajectory, for various infill patterns. Figure 2 displays the alterations in the nozzle trajectory resulting from changes in texture parameters for the rectilinear filling pattern. The nozzle path for a standard untextured sample is depicted in the top row as Figure 2a. The left column of the table depicts the nozzle trajectory for the rectilinear infill pattern with three protrusions. The protrusion offsets, as shown in Figure 2b–2d, are 0.25, 0.50, and 0.75 mm from top to bottom, respectively. In contrast, the right column illustrates the nozzle trajectories for six protrusions, with vertical offsets of 0.25, 0.50, and 0.75 mm, as depicted in Figure 2e–2g respectively.

The rectilinear infill pattern entails the parallel filling of material at a 45° angle, exhibiting a continuous

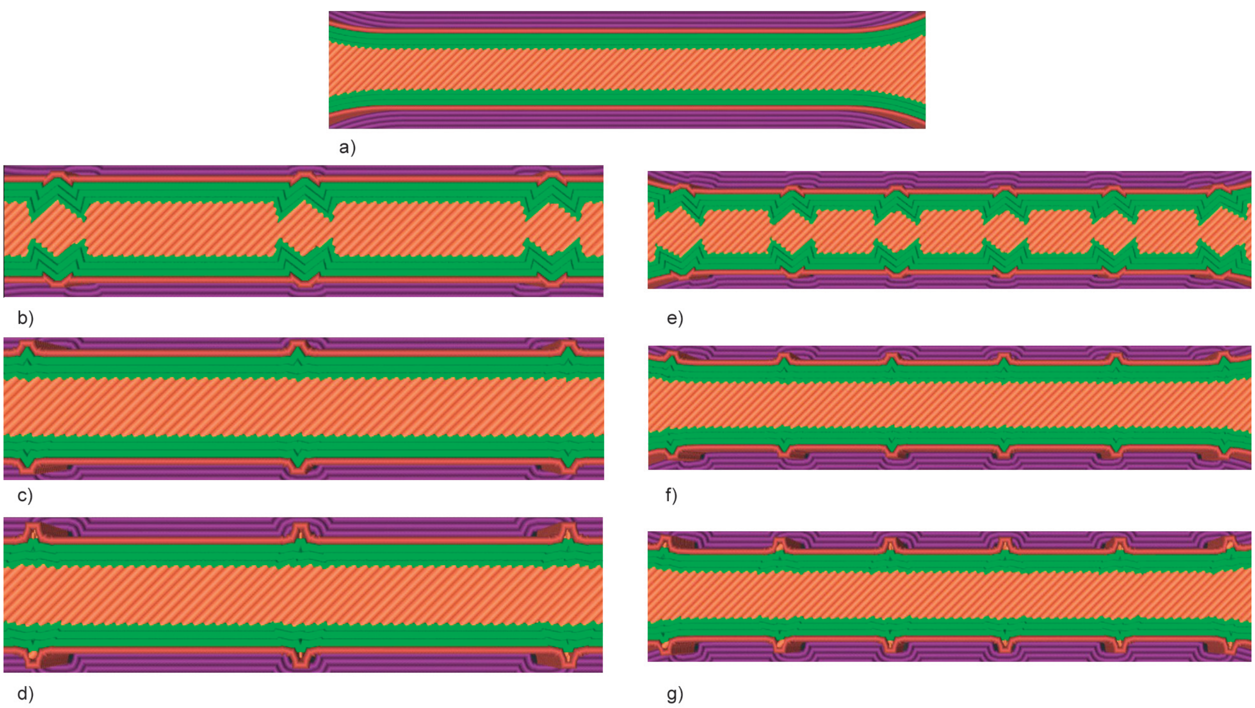


**Figure 2.** Slicing images of varying texture parameters for rectilinear infill pattern a) untextured sample, b) 3 protrusions 0.25 mm protrusion offset, c) 3 protrusions 0.50 mm offset, d) 3 protrusions 0.75 mm offset, e) 6 protrusions 0.25 mm, f) 6 protrusions 0.50 mm offset, g) 6 protrusions 0.75 mm offset.

pattern at corner turns during parallel transitions. In subsequent layers, the directional lines undergo a turning angle of 90°. In the case of the rectilinear pattern, it is noted that when the protrusion offset value is set to 0.25, the most pronounced alteration in the trajectory of both the wall and infill pattern is observed. The table highlights that the nozzle trajectory is similar for both cases when the protrusion offset is 0.50 and 0.75 mm.

Figure 3 displays the deviations in the nozzle trajectory resulting from changes in texture parameters for the line infill pattern. The top row displays the nozzle path for a typical untextured sample, as shown in Figure 3a. The table's left column shows the nozzle trajectory for the line infill pattern with three protrusions, with protrusion offsets of 0.25, 0.50, and 0.75 mm from top to bottom, as shown in Figure 3b–2d, respectively. In contrast, the right column depicts the trajectory for six protrusions, with offsets of 0.25, 0.50, and 0.75 mm in vertical sequence, as shown in Figure 3e–3g), respectively.

In the context of a line infill pattern, successive layers are deposited in parallel orientation at a 45° angle. Upon transitioning to the subsequent layer, a 90° rotation is executed concerning the lower layer. For the line pattern, it is observed that when the protrusion offset value is established at 0.25, the most substantial alternation in trajectory is discerned primarily for the wall, whereas the path of the infill pattern undergoes minimal alteration. However, it is observed that the nozzle trajectory is similar when the protrusion offset values are either 0.75 or 0.50 mm for the line infill pattern.

Figure 4 shows the changes in the nozzle path resulting from changes in texture parameters for the concentric pattern. The nozzle trajectory for a typical untextured sample is illustrated in the upper row as Figure 4a. The left column of the table shows the nozzle trajectory for the concentric infill pattern with three protrusions, featuring offsets of 0.25, 0.50, and 0.75 mm from top to bottom, as shown in Figure 4b–4d, respectively. Conversely, the right column illustrates the trajectory for six protrusions, with offsets of 0.25, 0.50, and 0.75 mm arranged in ascending order, as shown in Figure 4e–4g, respectively.

The concentric infill pattern adheres to the model's perimeter lines, gradually diminishing their dimensions as they approach the center. Regarding the concentric pattern, a considerable shift was observed in both the trajectory of the wall lines and the infill pattern trajectory, particularly notable when the protrusion length was fixed at 0.25 mm. Moreover, within the context of texture application to the specimens, this infill pattern exhibited the most pronounced

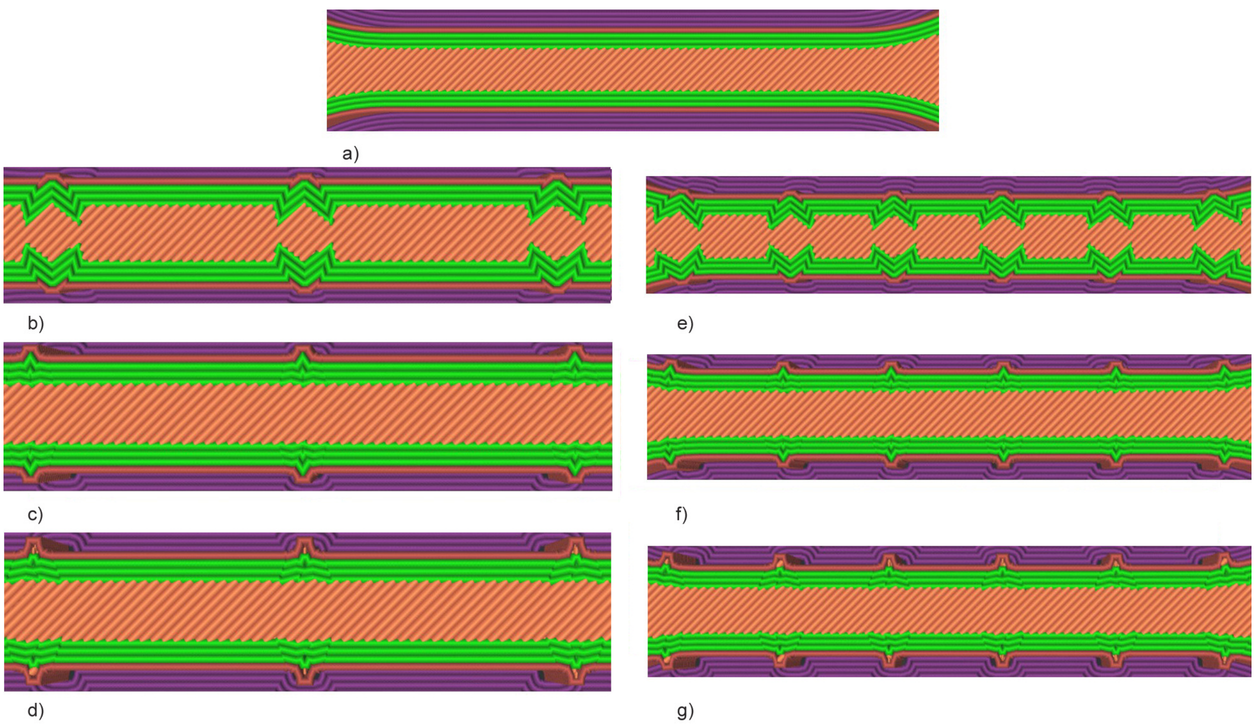


**Figure 3.** Slicing images of varying texture parameters for line infill pattern. a) Untextured sample, b) 3 protrusions 0.25 mm protrusion offset, c) 3 protrusions 0.50 mm offset, d) 3 protrusions 0.75 mm offset, e) 6 protrusions 0.25 mm, f) 6 protrusion 0.50 mm offset, g) 6 protrusions 0.75 mm offset.

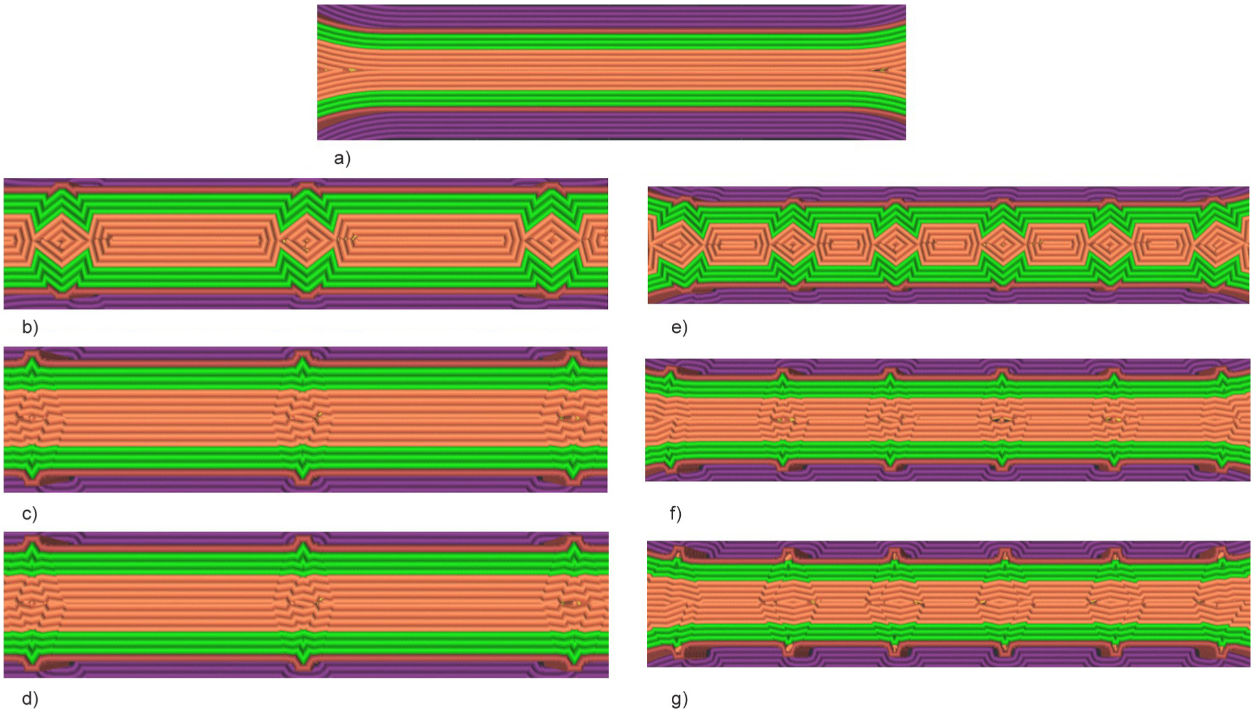


**Figure 4.** Slicing images of varying texture parameters for concentric infill pattern a) untextured sample, b) 3 protrusions 0.25 mm protrusion offset, c) 3 protrusions 0.50 mm offset, d) 3 protrusions 0.75 mm offset, e) 6 protrusions 0.25 mm, f) 6 protrusions 0.50 mm offset, g) 6 protrusions 0.75 mm offset.

trajectory alterations. When the protrusion offset is 0.75 and 0.50 mm, there is a noticeable difference in the nozzle trajectory for these two cases regarding the concentric infill parameter.

Within this research, parameters, including the number of protrusions employed in generating the texture, as well as the distance of the protrusion from the surface, were systematically altered. It is noteworthy that the overarching printing parameters remained constant for each individual case.

## 3. Results

### 3.1. Tensile test

This research investigated the influence of variations in nozzle path induced by texturing on the vertical surface of the material, with a focus on the resulting effect on mechanical strength. The mechanical properties of materials are evaluated through standardized tests, with the tensile test holding paramount importance among them. The experimental approach was to subject samples to a tensile test to assess their mechanical properties. In this study, 3 different infill patterns (rectilinear, line, concentric) were selected to fill the solid material. These infill patterns follow different trajectories while forming the interior of the material layer by layer. By applying texture to the materials, these trajectories were changed, and it was observed to what extent the mechanical properties of the materials changed with the change in the trajectory of the applied texture. Furthermore, the study examined how altering the size and quantity of textures affects the nozzle trajectory and, consequently, the mechanical properties of the sample. Ultimate tensile strength (UTS) values, obtained from the tensile test and representing the maximum stress materials can sustain before failure, play a crucial role in establishing structural design parameters. In engineering applications, the primary focus is on determining the maximum stress a material can endure prior to failure. Therefore, this study conducted a comparative analysis of the UTS values of the specimens. Figure 5 shows the ultimate tensile strengths of the specimens and the percentage decrease resulting from the texturing process compared to the untextured specimens. In the graphical representations of tensile test results, the specimen codes are shown at the $X$-axis and contain letters and numbers. The first letter corresponds to the initial letter of the filling pattern parameter of the sample, followed by numerical values indicating the number and dimensions of protrusions, thus providing a comprehensive labeling system for interpretation. The size of the protrusion is indicated by two numbers, where 25 represents 0.25 mm, 50 represents 0.50 mm, and

75 represents 0.75 mm. Figure 5 compares the change in ultimate tensile strength (UTS) for three infill patterns: rectilinear, line, and concentric. Figure 5a, Figure 5b, and Figure 5c illustrate the individual UTS changes for each pattern, respectively, while Figure 5d presents a comprehensive comparison. The first three plots contain dual *Y*-axes: the left *Y*-axis represents the ultimate tensile strength (UTS), while the right *Y*-axis indicates the percentage reduction in UTS compared to the untextured specimen for each texture case. These three graphs illustrate the variation in UTS for different texture parameters across three fill patterns: rectilinear, linear, and concentric, respectively. The fourth graph presents the percentage decrease in UTS, categorized by different texture parameters.

It was observed that the maximum tensile strength of the tensile specimens without texture was higher than that of the specimens with texture and that the UTS decreased accordingly with the infill pattern, size, and number of protrusions. The greatest reduction in ultimate tensile strength was observed for each infill pattern when the protrusion length was 0.25 mm, and the number of protrusions was 6. The observed phenomenon can be attributed to the significant deviation exhibited by the nozzle trajectory from its typical path during the process of texturing with a minor protrusion. The perturbation of the nozzle trajectory, contingent upon the dimensions and quantity of protrusions, alongside the infill configuration, is evident from the slicing representations delineated in Figure 2–5.

Another obvious trend is a slight decrease in mechanical properties for all infill patterns when the protrusion length is 0.50 mm. In particular, for the concentric pattern, a decrease in UTS of 2.36% was observed for 3 protrusions and 5.86% for 6 protrusions at this protrusion length, whereas for the texture created with the linear pattern, a decrease of 10.5% was observed for 3 protrusions and 14% for 6 protrusions at this protrusion length. The reason for this phenomenon is that the nozzle trajectory deviates slightly from the typical trajectory when a protrusion of this size is applied. It was observed that the ultimate tensile strength obtained at a protrusion length of 0.75 mm was lower than at a protrusion length of 0.50 mm and higher than at a protrusion length of 0.25 mm. At a protrusion length of

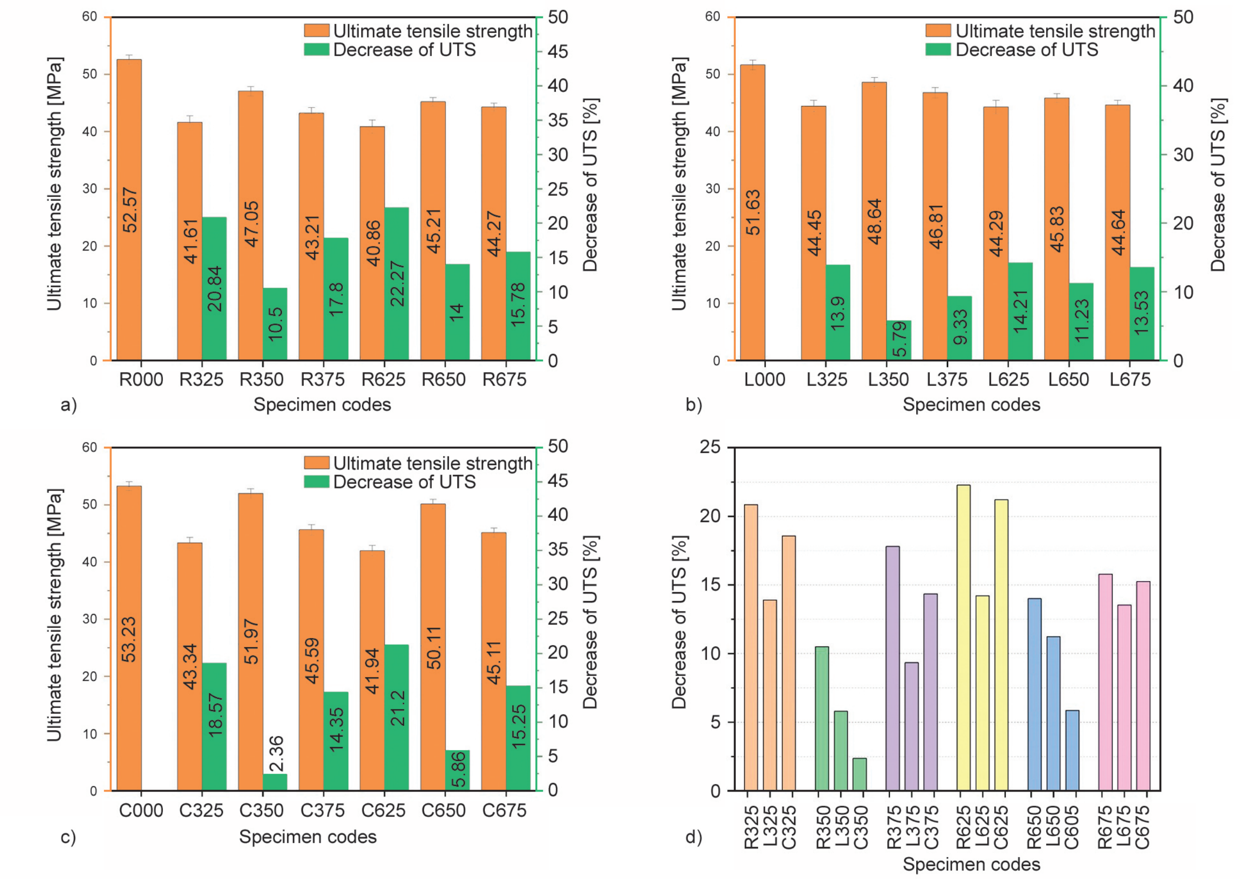


**Figure 5.** UTS variations for different infill patterns: a) rectilinear, b) line, c) concentric, and d) comprehensive comparison.

0.75 mm, a reduction in tensile strength was observed at this level due to the moderate deviation of the nozzle trajectory compared to the untextured trajectory.

It has been found that the offset of the protrusions used in texturing the part causes a change in the nozzle trajectory, and with this change, the ultimate tensile strength of the materials is inversely correlated with the change in trajectory. In addition, the increase in the number of protrusions caused a decrease in the ultimate tensile strength. The number of protrusions and the size of the protrusions were found to affect the different infill patterns in different ways.

## 3.2. Statistical analyses for factor evaluation

Statistical analyses are used to evaluate experimental results. The Taguchi method is a statistical analysis technique commonly used to evaluate the optimal level of each parameter in a system and determine the level of influence of the parameters on the result. It also considers the interaction of parameters. The method evaluates the experimental results by converting them into a signal-to-noise (S/N) ratio. The signal-to-noise ratio value is calculated and analyzed in different ways according to the target value of the experiment: smaller is better, larger is better, and nominal is better. In the study, the Taguchi method was used to analyze the effect of surface texture parameters on ultimate tensile strength. Since the target value is the ultimate tensile strength, for which larger values indicate better mechanical properties, larger is better was chosen for the signal-to-noise ratio. In order the perform the analysis, Minitab software was employed. The main factors considered were infill pattern, number of protrusions, and protrusion size, and the effect of these factors on ultimate tensile strength was analyzed.

The main effects plot for S/N ratio is shown in the Figure 6. It demonstrates that protrusion size has the greatest effect on UTS; pattern and number of protrusions have a similar effect and are very much smaller than the size effect on UTS. In general, the analysis shows that the highest UTS values are achieved when the protrusion size is 0.50 mm, the number of protrusions is 3, and the infill pattern is in concentric and line form.

Interaction plots are used for the analysis of interactions between factors. The software produces an interaction plot by plotting the characteristic mean for each combination of factor levels for the given factors.

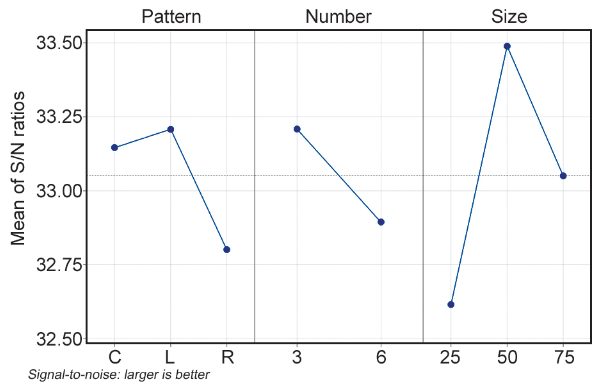


**Figure 6.** Main effects plot for S/N ratios.

If the lines are parallel or close to parallel, then there is no interaction between the factors; if the lines are not parallel, then there is an interaction between the two factors. The interaction plot for S/N ratios is shown in Figure 7.

Since the graph does not contain parallel curves, it is indicated that there is an interaction between the factors. In particular, there is a significant interdependence between protrusion size and infill pattern and a weak interaction between size and number of protrusions. Moreover, the factors are statistically meaningful. The graph shows all the factors that should be used to achieve optimum tensile strength. Furthermore, the combined effect of these factors on the UTS can be clearly seen in this graph.

## 3.3. Failure mechanism

Stress concentrations occur when there are irregularities in the geometry or material of a structural component that cause an interruption in the stress flow. This is caused by irregularities such as holes, grooves, notches and protrusions. Stress concentrations occur in the vicinity of these irregularities, and when the material is subjected to a force, greater stress occurs in these regions than in other areas,

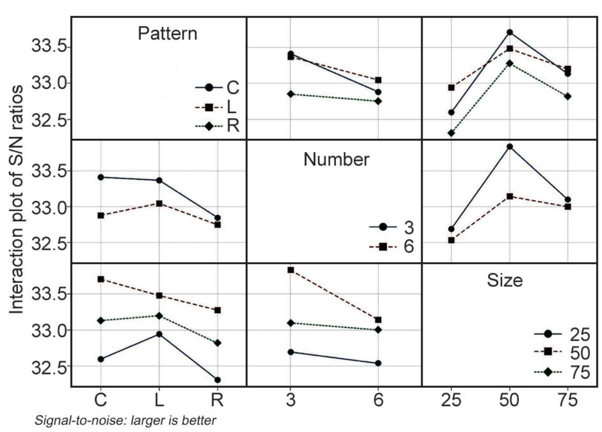


**Figure 7.** Interaction plot for S/N ratios.

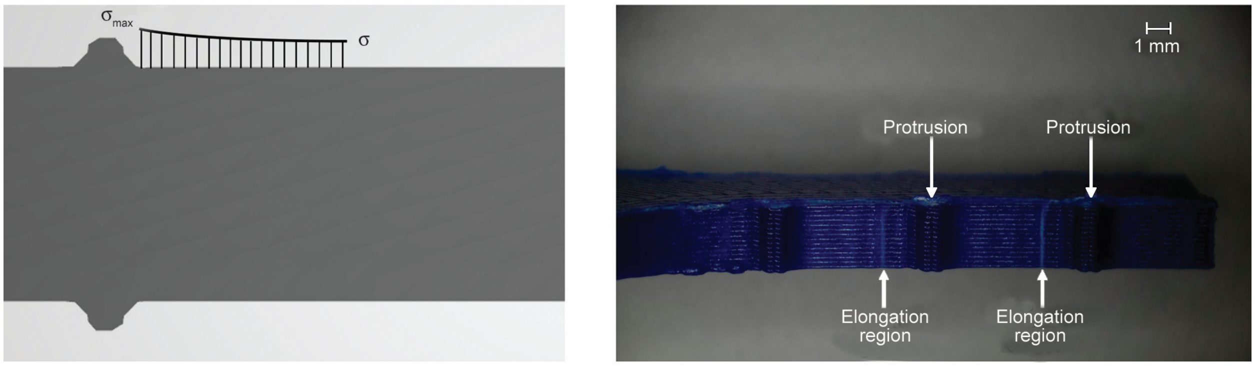


a) b)

**Figure 8.** Stress concentration regions a) stress distribution illustration, b) elongation regions.

and parts under load begin to damage from these areas. In this study, the protrusions create irregularities in the material, and the stress increases around the protrusions, as shown in Figure 8, and the specimens fractured around the protrusions in the tensile test.

Figure 8a was obtained by converting the G-code to STL format and is used to illustrate the increase in stress around the protrusion. Figure 8b presents a microscopic view of the sample after a tensile test has been applied to the textured sample, highlighting the elongation regions. In the stress concentration regions near the protrusions, the regions of specimen elongations are clearly visible as white vertical lines where maximum stress is applied.

In the analyses, it was found that the nozzle trajectory changed during the texturing process, which caused a decrease in the ultimate tensile strength of the object. Furthermore, the protrusions caused an increase in stress concentration, resulting in a decrease in the ultimate tensile strength of the specimen. It was observed that the deviation in the nozzle trajectories was similar in the production of specimens with 0.75 and 0.50 mm protrusion offset for the Line and Rectilinear infill patterns. However, the specimens with 0.75 mm protrusion offset failed at lower stresses due to a stress concentration effect. This is because the irregularity increases with protrusion offset. In addition, an increase in the number of protrusions resulted in a decrease in the ultimate tensile strength of the materials. This is because the stress concentration zones increased in certain regions, leading to material rupture at lower tensile stresses. This shows that in addition to the change in nozzle trajectory, the ultimate tensile strength is also influenced by the stress concentration. Figure 9 shows textured specimens after fracture, featuring a 0.5 mm protrusion offset for the line, rectilinear, and concentric infill patterns, as illustrated in Figure 9a, Figure 9b, and Figure 9c, respectively. These images clearly demonstrates that the specimens fractured from the stress concentration zones.

The effect of the stress concentration around protrusions in polymer additive manufactured materials on the tensile strength of the material should be determined by studies designed to do so. To carry out these studies, the tensile specimens should contain one protrusion, the geometry of this protrusion should be varied, and the tensile strength of the material should be correlated with the dimensional change of the irregularity. Further research is needed to have a better understanding of this effect.

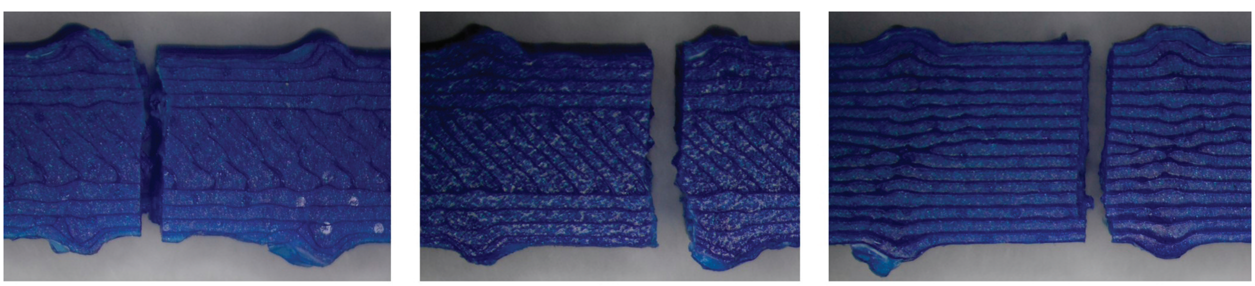

a) b) c)

**Figure 9.** Rupture images varying infill pattern 0.5 mm protrusion offset a) line, b) rectilinear, c) concentric.

## 4. Conclusions

This study examines the texture implementation method on the material during the production of 3D printer and influence of texturing parameters on the tensile strength of the material. In order to impart the customised texture to the specimen IdeaMaker slicing software was employed. The software generates the previously created black and white patterns on the vertical surface of the sample by indenting it in the *X-Y* axis. During this process, the software modifies the G-code in the *X-Y* axis and changes the nozzle trajectory used to create the wall and solid infill of the material. The parameters used in the texturing process were determined as the offset value of the protrusion in the *X-Y* plane, the number of protrusions, and the infill pattern used during this protrusion formation. The effect of the given specified parameters on the tensile strength of the material was analyzed by comparing the tensile test results of the textured and untextured specimens. The main findings of this study are that the mechanical strength of the material decreases with the texturing process, and the reason for this decrease is the deviation of the nozzle trajectory along the tensile plane during the printing of the infill pattern and wall layer of the textured sample. Slicing images that show the nozzle trajectory of the specimens and tensile test results were evaluated together, and it was observed that at 0.25 mm offset, where the change in nozzle trajectory was greatest, the tensile strength decreased by up to 22% depending on the infill pattern and at 0.50 mm offset, where the change in nozzle trajectory was minimum, a decrease of between 2 and 10% was observed depending on the infill pattern. At 0.75 mm offset, a moderate variation in the nozzle trajectory was observed, and a reduction in tensile strength between 9 and 17% was observed, depending on the infill pattern.

Statistical methods such as Taguchi analysis and Anova analysis were used to analyze the effects of surface texturing parameters on the ultimate tensile strength. In the texturing process, the largest effect on tensile strength was found to be the protrusion offset, and the effect of the number of protrusions and the infill pattern parameters on ultimate tensile strength was found to be of a similar magnitude and significantly less than the effect of protrusion size. In addition, the results were statistically meaningful, and the parameters were found to influence the results in a combined manner. From the statistical analysis of the tensile test results, it was found that choosing the protrusion offset of 0.5 mm, the number of protrusions as less, and the infill pattern as concentric and line will reduce the mechanical strength of the specimen less.

In addition, microscopic images of the specimens were examined after the tensile test, and it was observed that the fracture occurred at the corner of the protrusions. It was concluded that the reason for this was the formation of stress concentration at the corners of the protrusion. In the case of the 0.75 mm protrusion offset, the stress concentration at the corner of the protrusion is higher than in other cases, which explains why the specimens have lower mechanical strength than the 0.5 mm protrusion offset.

This behavior can be replicated similarly using various brands of PLA filaments and 3D printers, as texturing the materials results in alterations to their mechanical properties due to changes in nozzle trajectory and stress concentration, regardless of the brand of PLA or FFF-based 3D printer. Further studies in this field could investigate the effect of stress concentration caused by protrusion geometrical properties on material tensile strength. Furthermore, future studies could explore the outcomes of texturing materials using different filaments such as ABS, ASA, PETG, PC, and nylon. In addition, there is considerable potential in investigating the effect of various printing parameters on material texture. Among these parameters, 'line width' is expected to have a significant impact. This is due to the ability of smaller line widths to produce finer details and complex geometries, enabling high-resolution and precise texturing. This study is one of the early efforts in this area. The proposed future studies can be conducted to explore the limits of texturing with 3D printers.

## References

[1] Shaik Y. P., Schuster J., Shaik A.: A scientific review on various pellet extruders used in 3D printing FDM processes. Open Access Library Journal, **08**, e7698 (2021). https://doi.org/10.4236/oalib.1107698

[2] Mustapha K. B., Metwalli K. M.: A review of fused deposition modelling for 3D printing of smart polymeric materials and composites. European Polymer Journal, **156**, 110591 (2021). https://doi.org/10.1016/j.eurpolymj.2021.110591

[3] Krishnanand, Singh V., Mittal V., Branwal A. K., Sharma K., Taufik M.: Extrusion strategies in fused deposition additive manufacturing: A review. Proceedings of the Institution of Mechanical Engineers Part E: Journal of Process Mechanical Engineering, **238**, 988–1012 (2023). https://doi.org/10.1177/09544089221150709

[4] Kantaros A., Soulis E., Petrescu F. I. T., Ganetsos T.: Advanced composite materials utilized in FDM/FFF 3D printing manufacturing processes: The case of filled filaments. Materials, **16**, 6210 (2023). https://doi.org/10.3390/ma16186210

[5] Iftekar S. F., Aabid A., Amir A., Baig M.: Advancements and limitations in 3D printing materials and technologies: A critical review. Polymers, **15**, 2519 (2023). https://doi.org/10.3390/polym15112519

[6] Ganapathy S. B., Sakthivel A. R., Kandasamy J., Khan T., Aloufi M.: Optimization of printing process variables and the effect of post-heat treatments on the mechanical properties of extruded polylactic acid–aluminum composites. Polymers, **15**, 4698 (2023). https://doi.org/10.3390/polym15244698

[7] Coblas D. G., Fatu A., Maoui A., Hajjam M.: Manufacturing textured surfaces: State of art and recent developments. Proceedings of the Institution of Mechanical Engineers Part J: Journal of Engineering Tribology, **229**, 3–29 (2015). https://doi.org/10.1177/1350650114542242

[8] Curodeau A., Sachs E., Caldarise S.: Design and fabrication of cast orthopedic implants with freeform surface textures from 3-D printed ceramic shell. Journal of Biomedical Materials Research, **53**, 525–535 (2000). https://doi.org/10.1002/1097-4636(200009)53:5<525::AID-JBM12>3.0.CO;2-1

[9] Hong Y., Zhang P., Lee K-H., Lee C-H.: Friction and wear of textured surfaces produced by 3D printing. Science China Technological Sciences, **60**, 1400–1406 (2017). https://doi.org/10.1007/s11431-016-9066-0

[10] Holovenko Y., Antonov M., Kollo L., Hussainova I.: Friction studies of metal surfaces with various 3D printed patterns tested in dry sliding conditions. Proceedings of the Institution of Mechanical Engineers Part J: Journal of Engineering Tribology, **232**, 43–53 (2018). https://doi.org/10.1177/1350650117738920

[11] Jafari R., Cloutier C., Allahdini A., Momen G.: Recent progress and challenges with 3D printing of patterned hydrophobic and superhydrophobic surfaces. International Journal of Advanced Manufacturing Technology, **103**, 1225–1238 (2019). https://doi.org/10.1007/s00170-019-03630-4

[12] Ko K., Jin S., Lee S. E., Lee I., Hong J-W.: Bio-inspired bimaterial composites patterned using three-dimensional printing. Composites Part B: Engineering, **165**, 594–603 (2019). https://doi.org/10.1016/j.compositesb.2019.02.008

[13] Johnson A. A., Bingham G. A., Majewski C. E.: The design and assessment of bio-inspired additive manufactured stab-resistant armour. Virtual and Physical Prototyping, **13**, 49–57 (2018). https://doi.org/10.1080/17452759.2017.1369438

[14] Mai J., Thistleton C., Löschke S. K., Proust G., Dong A.: Towards a new techno-aesthetic paradigm: Experiments with pattern, texture and colour in 3D-printed wood-plastic composites. in 'Proceedings of the 27$^{th}$ Annual International Solid Freeform Fabrication Symposium – An Additive Manufacturing Conference, Austin, USA' 1868–1877 (2016).

[15] Ou J., Dublon G., Cheng C-Y., Ishii H.: Cilllia: Method of 3D printing micro-pillar structures on surfaces. in 'Fabricate' (eds.: Menges A., Sheil B., Glynn R., Skavara M.), UCL Press, London, 184–189 (2019). https://doi.org/10.2307/j.ctt1n7qkg7.29

[16] van Rompay T. J. L., Finger F., Saakes D., Fenko A.: 'See me, feel me': Effects of 3D-printed surface patterns on beverage evaluation. Food Quality and Preference, **62**, 332–339 (2017). https://doi.org/10.1016/j.foodqual.2016.12.002

[17] Maekawa K., Hayashi T., Watanabe Y.: Design and rapid prototyping of affective shapes with 1/f fluctuation characteristics. in 'Proceedings of the 6$^{th}$ Asian Design International Conference, Tsukuba, Japan' 1–9 (2003).

[18] Armillotta A.: Assessment of surface quality on textured FDM prototypes. Rapid Prototyping Journal, **12**, 35–41 (2006). https://doi.org/10.1108/13552540610637255

[19] Jee H., Sachs E.: Surface macro-texture design for rapid prototyping. Rapid Prototyping Journal, **6**, 50–59 (2000). https://doi.org/10.1108/13552540010309877

[20] Zhou S., Jiang C., Lefebvre S.: Topology-constrained synthesis of vector patterns. ACM Transactions on Graphics, **33**, 215 (2014). https://doi.org/10.1145/2661229.2661238

[21] Dumas J., Lu A., Lefebvre S., Wu J., Dick C.: By-example synthesis of structurally sound patterns. ACM Transactions on Graphics, **34**, 137 (2015). https://doi.org/10.1145/2766984

[22] Kobayashi Y., Shirai K.: Multi-axis milling for microtexturing. International Journal of Precision Engineering and Manufacturing, **9**, 34–38 (2008).

[23] Yaman U., Dolen M., Hoffmann C.: Generation of patterned indentations for additive manufacturing technologies. IISE Transactions, **51**, 209–217 (2019). https://doi.org/10.1080/24725854.2018.1491076

[24] Weinhaus F. M., Devarajan V.: Texture mapping 3D models of real-world scenes. ACM Computing Surveys, **29**, 325–365 (1997). https://doi.org/10.1145/267580.267583

[25] Zharylkassyn B., Perveen A., Talamona D.: Effect of process parameters and materials on the dimensional accuracy of FDM parts. Materials Today: Proceedings, **44**, 1307–1311 (2021). https://doi.org/10.1016/j.matpr.2020.11.332